Iron isotopes reveal distinct dissolved iron sources and pathways in the intermediate versus deep Southern Ocean

Cyril Abadie[a], Francois Lacan[a,1], Amandine Radic[a], Catherine Pradoux[a], and Franck Poitrasson[b]

[a]LEGOS, University of Toulouse, CNRS, CNES, IRD, UPS, 31400 Toulouse, France; and [b]Géosciences Environnement Toulouse, UMR 5563 CNRS/UPS/IRD, 14-16 avenue Edouard Belin, 31400 Toulouse, France

Edited by Donald E. Canfield, Institute of Biology and Nordic Center for Earth Evolution, University of Southern Denmark, Odense M, Denmark, and approved December 13, 2016 (received for review February 24, 2016)

As an essential micronutrient, iron plays a key role in oceanic biogeochemistry. It is therefore linked to the global carbon cycle and climate. Here, we report a dissolved iron (DFe) isotope section in the South Atlantic and Southern Ocean. Throughout the section, a striking DFe isotope minimum (light iron) is observed at intermediate depths (200–1,300 m), contrasting with heavier isotopic composition in deep waters. This unambiguously demonstrates distinct DFe sources and processes dominating the iron cycle in the intermediate and deep layers, a feature impossible to see with only iron concentration data largely used thus far in chemical oceanography. At intermediate depths, the data suggest that the dominant DFe sources are linked to organic matter remineralization, either in the water column or at continental margins. In deeper layers, however, abiotic non-reductive release of Fe (desorption, dissolution) from particulate iron—notably lithogenic—likely dominates. These results go against the common but oversimplified view that remineralization of organic matter is the major pathway releasing DFe throughout the water column in the open ocean. They suggest that the oceanic iron cycle, and therefore oceanic primary production and climate, could be more sensitive than previously thought to continental erosion (providing lithogenic particles to the ocean), particle transport within the ocean, dissolved/particle interactions, and deep water upwelling. These processes could also impact the cycles of other elements, including nutrients.

iron isotopes | GEOTRACES | South Atlantic | Southern Ocean | remineralization

Since the discovery that Fe is a limiting factor for phytoplankton growth (1), numerous studies have attempted to better constrain its cycle, sources, and sinks, and the processes occurring within the water column. Although atmospheric dust dissolution has long been thought to be the main source of dissolved iron (DFe) to the open ocean, the last decade has seen numerous studies suggesting other potential sources of DFe to the ocean. These include dissolution and/or desorption from continental margin sediments with or without Fe reduction, riverine inputs, and hydrothermalism (2).

Whereas the oceanic iron cycle is partially controlled by biological processes, it is, unlike major nutrients, widespread in the water column in the particulate form, notably as lithogenic particulate iron. It is a particle-reactive element, sensitive to scavenging processes (i.e., adsorption/desorption onto/from sinking particles). Recent work suggests continuous exchange between the dissolved and particulate iron phases (3, 4), as previously proposed for thorium and protactinium (5), rare earth elements (6), and copper (7). The relative importance of these organic and inorganic processes in the control of the iron cycle remains largely unknown, however, thereby restricting the validity of oceanic biogeochemical modeling involving this element and thus its use in ocean research.

Iron isotopes have emerged as a new powerful tool to constrain the Fe sources and oceanic cycle (3, 4, 8–17). The isotopic signatures of the various iron sources to the ocean are summarized in Fig. 1. It can be inferred from these diverse signatures that iron isotopes will bring new constraints on DFe sources to the ocean. In addition, several processes involved in the iron cycling within the water column (e.g., biological uptake, remineralization, scavenging, adsorption, desorption, dissolution, precipitation, organic complexation, and redox processes) may fractionate iron isotopes (14, 18–22). Hence, such isotopic fractionations may also bring additional constraints on the iron cycle within the water column.

Few existing studies report dissolved δ^{56}Fe [δ^{56}DFe, expressed here as the ^{56}Fe/^{54}Fe ratio relative to the Institute for Reference Materials and Measurements (IRMM)-014 reference material] values in the open ocean. Dissolved δ^{56}Fe ranges from −0.13 to +0.21 ± 0.08‰ in the Southeastern Atlantic (8), from −1.35 ± 0.03‰ to +0.80 ± 0.06‰ in the North Atlantic (4, 11), and from −0.03 ± 0.07‰ to +0.58 ± 0.08‰ in the Equatorial Pacific (3, 10). However, there is a lack of iron isotope data in high-nutrient low-chlorophyll (HNLC) areas, despite the fact that iron plays a critical role in these areas where it limits primary production. Here, we report a section of DFe isotopic compositions in the South Atlantic and Southern Ocean. Its dominant feature is a striking DFe isotopic minimum (light DFe, ranging from −0.17 to −0.74‰) found at intermediate depth (200- to 1,300-m depth), all along the section from the subtropical domain to the Weddell Gyre, contrasting with heavier DFe in the deeper layers.

Significance

Iron is an essential micronutrient for life. However, its scarcity limits algae growth in about one-half of the ocean. Its cycle is therefore linked to the global carbon cycle and climate. We present an iron isotope section from the Southern Ocean. In contrast to the common but oversimplified view, according to which organic matter remineralization is the major pathway releasing dissolved iron below the surface layers, these data reveal other dominant processes at depth, likely abiotic desorption/dissolution from lithogenic particles. This suggests that the iron cycle, and therefore primary production and climate, may be more sensitive than previously thought to continental erosion, dissolved/particle interactions, and deep water upwelling. These processes likely impact other elements in the ocean.

Author contributions: F.L. designed research; C.A., F.L., and A.R. performed research; C.A., F.L., A.R., and C.P. contributed new reagents/analytic tools; C.A., F.L., A.R., and F.P. analyzed data; and C.A., F.L., and F.P. wrote the paper.

The authors declare no conflict of interest.

This article is a PNAS Direct Submission.

Data deposition: The data have been deposited in the GEOTRACES database, www.egeotraces.org/.

[1]To whom correspondence should be addressed. Email: francois.lacan@legos.obs-mip.fr.

This article contains supporting information online at www.pnas.org/lookup/suppl/doi:10.1073/pnas.1603107114/-/DCSupplemental.

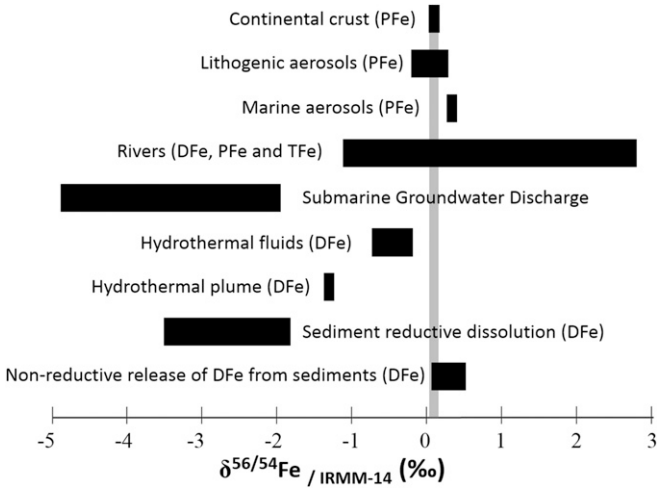

Fig. 1. Isotopic composition of iron sources to the ocean (in per mill relative to IRMM-014). DFe, PFe, and TFe stand for dissolved, particulate, and total iron, respectively. References used in the figure are as follows: continental crust (49); lithogenic aerosols (50); marine aerosols (3); rivers (ref. 51 and references therein); submarine groundwater discharges (52); hydrothermal fluids (53); hydrothermal plumes (11); sediment reductive dissolution (9, 12); non-reductive release of DFe from sediments (3, 10, 17).

This pattern, invisible to iron concentrations, demonstrates contrasted DFe origins in these different layers. We suggest that, although biological material remineralization processes dominate at intermediate levels, non-reductive release of DFe from particles (notably lithogenic ones) dominates in the deep ocean.

Samples for this study were collected on board the French R/V *Marion Dufresne* from February 8 to March 24, 2008 in the Atlantic sector of the Southern Ocean, which partly lies within a HNLC area, during the Bonus/GoodHope (BGH) cruise (GEOTRACES cruise GIPY4). Fig. 2 shows the studied area, with the five stations where the samples were collected, together with the main oceanographic fronts and currents. The section crosses the Antarctic Circumpolar Current (ACC), which is the world's largest current. It is therefore located in a highly dynamic area. A detailed description and understanding of the currents and the water masses they carry is therefore absolutely essential for data interpretation. Accordingly, before comparing the Fe isotopic compositions of the different samples, we first need to ensure that these may be related to each other, either because they belong to the same water mass (i.e., the same reservoir), or because the different water masses to which they belong are related through mixing processes.

Apart from the Agulhas Current carrying waters from the Indian Ocean westward—the Indian influence being observed down to ~1,500-m depth (23)—the flows across the section are dominated by eastward currents, the ACC and the Northern limb of the Weddell Gyre (24). Superimposed on this intense zonal circulation, there is a slow meridional and vertical circulation, schematized in Fig. 2. Its effects are clearly visible from meridional sections of water mass tracers, such as salinity and dissolved oxygen concentrations shown in Fig. 3. The hydrographic properties, potential temperatures, salinities, and dissolved O_2 concentrations from the five stations, highlighting the main samples and water masses discussed below, are displayed in Fig. 3 and Fig. S1.

Results

DFe concentrations and isotopic compositions are shown in Figs. 3 and 4 (and Fig. S2 and Dataset S1; these data are also available from the GEOTRACES database; www.egeotraces.org/). Concentrations range from 0.05 to 0.89 nmol·kg^{-1}. They tend to decrease from north to south with maximum values in S1 close to the African margin, minimum values in S4 in the ACC, and then

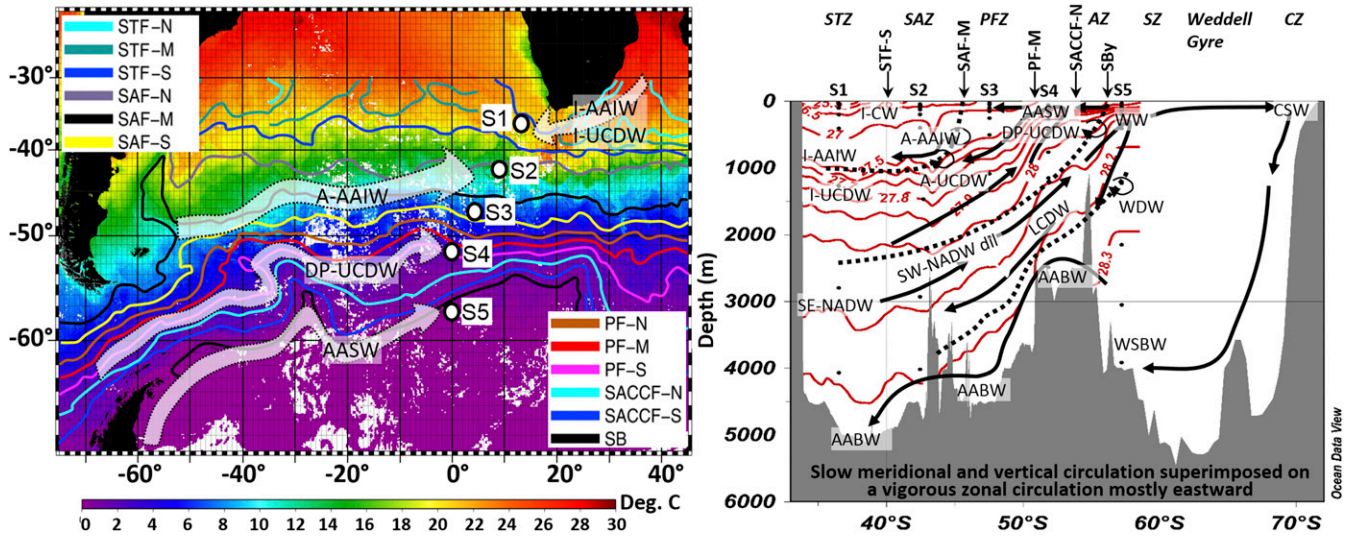

Fig. 2. Studied area. (*Left*) Background colors indicate sea surface temperatures (14-d average centered on March 1, 2008, MODIS data; map produced by the Colorado Center for Astrodynamics Research, data viewer using data from the Group for High Resolution Sea Surface Temperature). S1 to S5 are the five sampled stations. Colored lines indicate front locations, from ref. 54. Arrows schematize the trajectories of the water masses in which the DFe isotope minima were found. (*Right*) Schematic representation of the meridional and vertical circulation in the Southern Ocean adapted from Talley et al. (24). Front locations, zones, and water masses are indicated. Neutral density isolines (γ) (in kilograms per cubic meter) from the BGH cruise are shown in red. Sample locations are shown by black dots. Acronyms: AABW, Antarctic Bottom Water; AASW, Antarctic Surface Water; AZ, Antarctic Zone; CSW, Continental Shelf Water; CZ, Continental Zone; I-AAIW and A-AAIW, Antarctic Intermediate Water of Indian and Atlantic origins; I-CW, Indian Central Water; I-UCDW, A-UCDW, and DP-UCDW, Indian, Atlantic, and Drake Passage Upper Circumpolar Deep Water; LCDW, Lower Circumpolar Deep Water; -M, middle branch; -N, northern branch; PF, Polar Front; PFZ, Polar Frontal Zone; -S, southern branch; SACCF, southern ACC front; SAF, Sub-Antarctic Front; SAZ, Sub-Antarctic Zone; SB, southern boundary of the ACC; SE-NADW and SW-NADW, Southeast and Southwest North Atlantic Deep Water (dil, diluted); STF, Subtropical Front; STZ, Subtropical Zone; SZ, Southern Zone; WDW, Warm Deep Water; WSBW, Weddell Sea Bottom Water; WW, Winter Water.

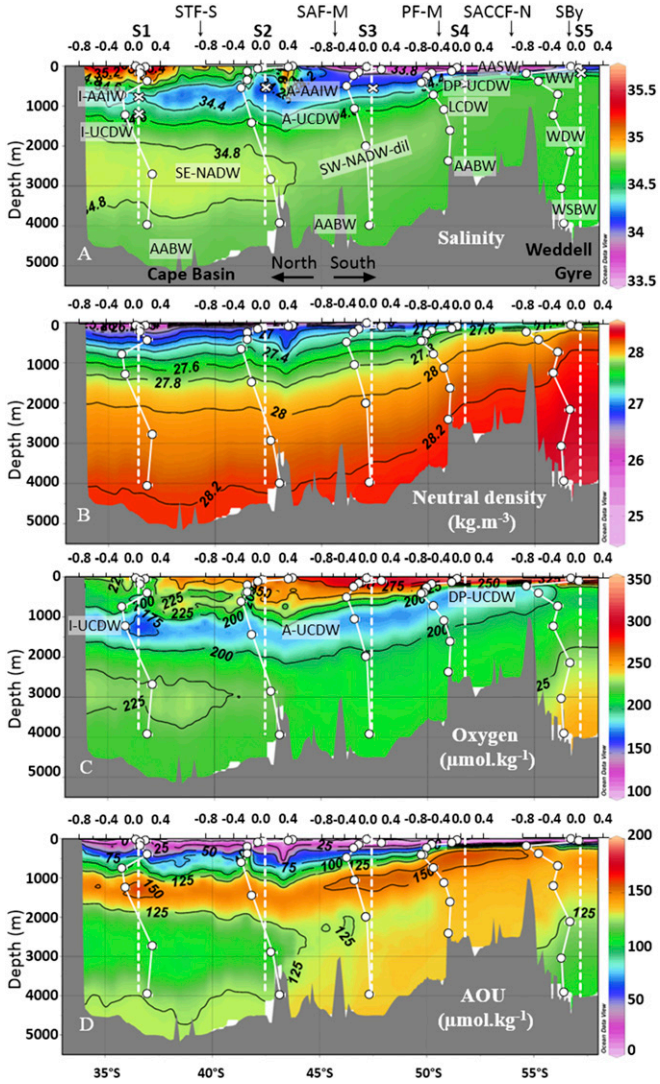

Fig. 3. DFe isotopic compositions profiles (δ^{56}DFe relative to IRMM-14 in per mill) plotted above sections of salinity (*A*), neutral density (in kilograms per cubic meter) (*B*), dissolved oxygen (in micromoles per kilogram) (*C*), and AOU (in micromoles per kilogram) (*D*) for seawater samples taken during the BGH cruise (stations S1 to S5). White circles are δ^{56}DFe data corresponding to the scale shown above each depth profile. Dashed white lines represent the δ^{56}Fe composition of the crust (0.07‰) (49) and the positions of the stations. At each station, salinity, neutral density, dissolved oxygen, and AOU have to be read on the dashed white lines and not at the positions of the white circles. White crosses show the positions of the δ^{56}DFe minimum at each station. Front positions are indicated. See Fig. 2 for acronyms. Figure was made using Ocean Data View (55).

increase again in station S5 in the Weddell Gyre. Profiles of DFe display a typical nutrient-like shape, with a surface minimum and an increase with depth. DFe isotopic compositions range from −0.74 to +0.47‰. The δ^{56}DFe values become more negative when going from the subtropical domain in S1 to the south in the ACC domain (S4). These δ^{56}DFe negative values remain in the Weddell Gyre, in S5. At each station, and in contrast to the quasi-monotonous increase of Fe concentrations with depth, a prominent δ^{56}DFe vertical minimum is found at intermediate depths (Figs. 3 and 4, and Fig. S2). The samples where this minimum is found are indicated by red diamonds in the diagram in Fig. S1. This diagram highlights the different water masses carrying this signal: different varieties of Antarctic Intermediate Water (AAIW) and Upper Circumpolar Deep Water (UCDW) originating from the Indian Ocean at station S1 and from the west at stations S2–S3–S4, and at station S5 a subsurface variety (205 m) of Antarctic Surface Water (AASW), called Winter Water.

Discussion

Origin of the δ^{56}DFe Minimum at Intermediate Depths. A prominent feature of our dataset lies with the abovementioned δ^{56}DFe minimum at intermediate depths ranging from −0.74 to −0.71‰ in S5 and S4 to −0.17‰ in S1 (Figs. 3 and 4, and Fig. S2). This feature has not been seen so far in the few other oceanic regions where δ^{56}DFe studies have been conducted, notably in the North Atlantic (11) and in the Equatorial Pacific (3, 10). These variations are not matched and therefore could not have been hinted at by the concentration profiles.

Redox processes are known to exert a major control on iron isotope compositions with reduced iron favoring light Fe isotope compositions (e.g., ref. 25). Measurements of DFe redox speciation (DFe^{II} and total DFe from which DFe^{III} can be computed) during the BGH cruise provide the opportunity to evaluate the effect of the iron redox state on its isotope signature in the open ocean. These data show that Fe(II) accumulation mostly occurs close to the surface, but not at intermediate depths (26). This mismatch between measured iron redox state and isotopic composition demonstrates that local iron reduction—at the time and location of sampling—was not responsible for the observed intermediate depth δ^{56}DFe minimum. This does not imply that redox processes could not have contributed to the observed minima. Iron reduction followed by reoxidation could lead to the observed signals. In such a case, these redox speciation data imply that these redox processes must have occurred before sampling, that is, upstream, remotely. This could come from the external DFe sources (e.g., at the ocean interfaces), or within the water masses (including dissolved/particle interactions), again upstream of the sampling location. In the following discussion, we will first explore the potential role played by water mass transport and mixing of signals acquired within the water column, and then the potential impact of external sources.

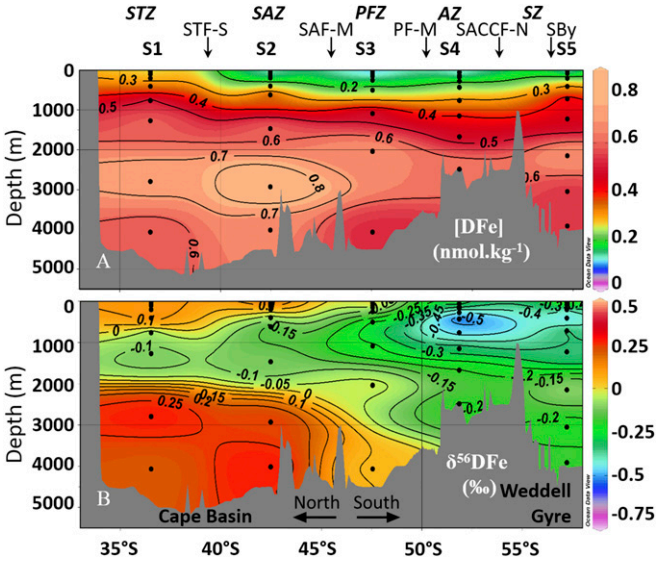

Fig. 4. Sections of (*A*) DFe concentrations ([DFe] in nanomoles per kilogram) and (*B*) DFe isotopic composition (δ^{56}DFe relative to IRMM-14 in per mill) of seawater samples taken during the BGH cruise (black dots). Fronts locations are indicated. See Fig. 2 for acronyms. Figure was made using Ocean Data View (55).

Although the circulation across the section is mainly zonal and structured along circumpolar fronts, meridional water mass transports do occur across these fronts as reflected, for instance, by salinity and oxygen meridional sections (Fig. 3). These meridional transports occur mainly along isopycnal surfaces. Neutral density isolines from the BGH section are displayed in Fig. 2 superimposed on the schematic meridional circulation adapted from Talley et al. (24). The isopycnal distribution is in very good agreement with the circulation scheme described by Talley et al., which confirms that this scheme may be used to describe the meridional circulation that impacts the BGH section. In addition to this information, a detailed examination of the sample hydrographic properties (θ, *S*, [O_2], nutrients) is used in the following to relate the different samples to each other.

Stations S2, S3, and S4 are all located within the ACC. Their intermediate and deep waters all originate from the west and the Drake Passage. They form a coherent group of stations, which we will discuss first. The AAIW sampled at stations S2 and S3 is formed by subduction of AASW that itself results from the upwelling of UCDW (24, 27, 28). The δ^{56}DFe minimum found in the AAIW of S2 and S3 may therefore originate from the dilution of the S4 UCDW δ^{56}DFe minimum through mixing with AASW. A simple two end-member mixing calculation illustrated in Fig. 5 clearly confirms this hypothesis.

Furthermore, the Atlantic AAIW sampled at stations S3 and S2 (Fig. 2) flows eastward into the Indian Ocean where it is further modified to form Indian AAIW, part of which returns to the Atlantic just south of South Africa, where we sampled it at station S1 (Fig. 2). Similarly, the Winter Water and Warm Deep Water where the δ^{56}DFe minimum is found at S5 are formed from AASW that itself results from the upwelling of UCDW (24, 27). Therefore, the circulation and water mass formation in the Southern Ocean suggest that the S4 UCDW light isotopic signature could also contribute to the δ^{56}DFe minima observed at stations S1 and S5. There are significant hydrographical property (θ, *S*, [O_2]) differences between the water masses in which the δ^{56}DFe minima were found (Fig. S1) at stations S1 and S5, compared with S2–S3–S4. These differences cannot be quantitatively addressed in the present case because (*i*) we lack iron isotope data in the Indian Ocean and Weddell Sea that would be required for mixing calculations, (*ii*) S1 and to a lesser extent S5 are under the clear influence of lithogenic inputs (29), and (*iii*) S5 is under the influence of surface processes, air/sea fluxes, and biology.

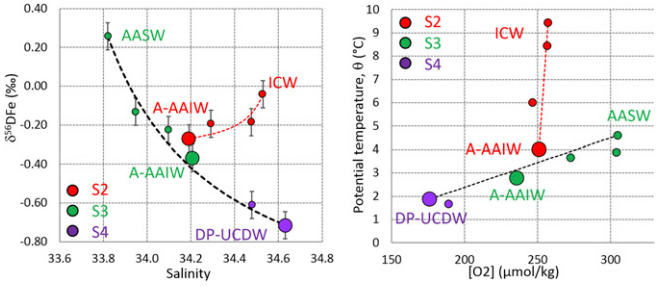

Fig. 5. Mixing diagrams. Properties of the Drake Passage Upper Circumpolar Deep Water (DP-UCDW), Atlantic Antarctic Intermediate Water (A-AAIW), Antarctic Surface Waters (AASW), and Indian Central Water (ICW) are shown for stations S2, S3, and S4. The dotted lines denote the theoretical conservative mixing curves between DP-UCDW and AASW (black dotted line) and A-AAIW and ICW (red dotted line; see *Supporting Information* for the mixing equations). The large symbols identify the δ^{56}DFe minimum sample at each station. The diagrams show that the A-AAIW properties can be explained by a mixing between DP-UCDW and AASW. The slight deviation of the S2 A-AAIW properties from this mixing (black dotted line) is explained by a small contribution of the warm and salty Indian Central Water (red).

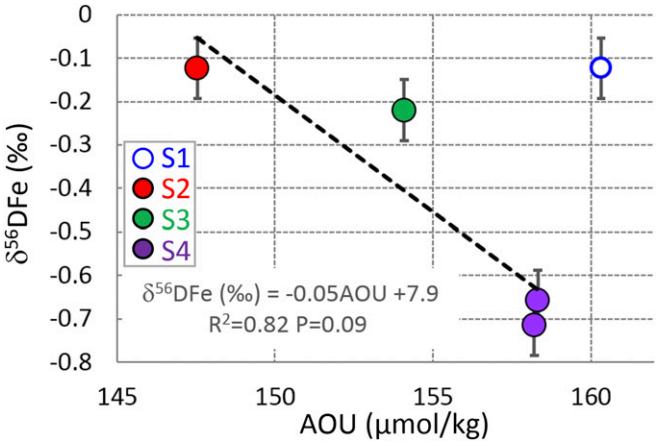

Fig. 6. Dissolved iron isotopic composition of the different varieties of UCDW as a function of AOU. The dotted line shows the linear regression calculated excluding the Indian UCDW of station S1 that is significantly impacted by lithogenic inputs from the South African margin. S5 is not shown because there is no UCDW at this station.

The above discussion shows that the light isotopic signature of the UCDW variety sampled at station S4—namely, the Drake Passage UCDW—is the source of the intermediate δ^{56}DFe minimum found throughout the ACC (S2–S3–S4) and could also impact S1 and S5. The UCDW is characterized by an oxygen minimum and a maximum in apparent oxygen utilization (AOU) (24). These characteristics result from the accumulation (integration) of organic matter remineralization (that consumes oxygen) occurring within the water mass as it ages. It is higher in this water mass compared with the surrounding waters. The isotopic fractionations associated with organic matter remineralization processes have not yet been extensively constrained. However, remineralization could potentially release light iron through kinetic fractionation, or from an initially light signature of the remineralized matter [two studies suggest a preferential uptake of light Fe isotopes by phytoplankton (10, 14), although adsorption experiments on phytoplankton lead to the opposite conclusion (30)], or from reduction steps involved in several remineralization mechanisms [e.g., grazing (31), microbial reduction in aggregates (32)]. These light signatures could then be redistributed meridionally across the ACC as explained above.

Other types of UCDW have been sampled: the Indian UCDW at station S1 (1,721 m, δ^{56}DFe = –0.12‰) and the Atlantic UCDW at stations S2 and S3 (δ^{56}DFe = –0.12 and –0.22‰, respectively). They are also characterized by an oxygen minimum and an AOU maximum (reflecting remineralization within the water column). They all display light δ^{56}DFe values, just slightly heavier than the overlying AAIW (Fig. 3). This confirms that, in this area, high remineralization coincides with light DFe isotope signature. The UCDW δ^{56}DFe values are plotted versus AOU in Fig. 6. Excluding station S1, under the influence of lithogenic inputs, a trend can be seen: the higher the AOU, the more negative the δ^{56}DFe. This supports the conclusion according to which remineralization within the water column is the most likely origin of the light isotopic signatures found in the UCDW, which are then transferred to AAIW at least in the ACC domain (stations S2–S3–S4).

Remineralization of organic matter likely plays an additional role in the observed intermediate isotope minimum. At some oceanic margins, bacterial organic matter remineralization leads to anoxic conditions in the sediments due to bacterial respiration. These anoxic conditions lead to the reduction of Fe(III) into soluble Fe(II), which is transferred to the water column. There, iron is rapidly reoxidized but nevertheless keeps a light isotopic signature (9, 12, 13, 16). Such sources may contribute to the observed δ^{56}DFe

minimum especially in S1 and S5 [clearly influenced by margin inputs (29)], and to a lesser extent also within the ACC.

About 5% of the AAIW flowing in the Agulhas Current originate as Red Sea Water [the equivalent of ∼1 Sv of pure Red Sea Water (33)]. This water mass is associated to an extreme oxygen minimum originating in the northern Arabian Sea (33), where elevated Fe(II) concentrations have been reported (34). Therefore, very light Fe isotopic signatures resulting from reductive processes in the remote Arabian Sea, could, despite significant erosion due to water mass mixing along the way, contribute to the intermediate δ^{56}DFe minimum found at S1 in the Indian AAIW. The Red Sea Water DFe isotopic composition has not been documented yet. If we assume that it is characterized by a δ^{56}DFe value of −3‰ [such as what is observed in the Californian oxygen minimum zone (9)] and a DFe concentration 60% larger than that of the surrounding waters with which it would mix, and assuming a crustal isotopic composition for these surrounding waters (δ^{56}DFe = +0.07‰), then the mixing of 5% Red Sea Water with 95% surrounding waters would lead to the δ^{56}DFe value of −0.17‰ measured in the Indian AAIW sampled at S1. This shows that the above scenario is realistic. Similarly, large organic matter accumulation rates in the Antarctic Peninsula margin sediments, leading to reducing environments, have been shown to supply DFe through reductive dissolution (35). This could contribute to the negative DFe isotopic signature found at station S5. The impact of matter inputs from the margins of South Africa and the Antarctic Peninsula is supported by several other geochemical studies, based on rare earth element concentrations and Nd isotopic compositions (29, 36), Pb, Cu, Ag, and Co concentrations (23, 37), and Fe physical speciation (38).

In summary, the above discussion suggests that remineralization of particulate organic matter within the water column imparts to the UCDW light DFe isotopic signatures, which are transferred to the Antarctic Intermediate Water through mixing especially in the ACC domain. In addition, remineralization of organic matter at the continental margins leads to the release of isotopically light DFe through reductive sediment dissolution, which likely also contributes to the intermediate water light isotopic signatures, especially at the northernmost and southernmost stations S1 and S5. The conjunction of both processes likely explains the observed δ^{56}DFe intermediate minimum all along the BGH section.

Processes Releasing DFe in the Deep Southern Ocean. The intermediate δ^{56}DFe minimum contrasts with more positive values found at the surface and in the deep layers (Figs. 3 and 4, Fig. S2, and Dataset S1). The surface layer is potentially subjected to multiple external sources and processes, notably dust depositions, phytoplankton uptake, and photoreduction that may affect DFe isotope composition and will not be discussed further. Below this surface layer, it is commonly thought that competition between one release process, remineralization of organic matter, and one sink, scavenging, acts as the major control on DFe vertical distributions (2, 39–41).

However, the clear contrast between the intermediate and deep δ^{56}DFe signatures along the BGH section (Figs. 3 and 4) goes against this paradigm. It reveals that distinct in situ processes and/or external sources dominate the DFe cycle at these two depths. With the assumption that the DFe sink at both depths (intermediate and deep) is dominated by the same scavenging process (2, 39, 40), then our observations suggest that the processes dominating the DFe sources in the deep ocean layers are not organic matter remineralization given the heavier DFe isotopic signatures uncovered. At depth, non-reductive release of DFe from particles (3, 10, 11, 17) could produce the observed isotopically heavier DFe, potentially through the following: (*i*) desorption as suggested for thorium and protactinium (5), rare earth elements (6) or copper (7), or (*ii*) ligand (siderophore)-promoted dissolution (42). This hypothesis is supported by the recent documentation of the isotopic signature of a labile fraction of suspended particles (from the North Atlantic), for which typical values are found around −0.3‰ (43). Adding to this value an isotopic fractionation associated to non-reductive release, typically characterized by $\Delta^{56}Fe_{\text{DFe-PFe}} \sim +0.3$‰ (3, 10), could lead to continental crust-like deep isotopic signatures observed for DFe along our transect, with values from −0.35 to +0.28‰ (Figs. 3 and 4). The particulate phases potentially involved in these processes could include both organic and inorganic particles, among which are erosion products, notably from atmospheric and riverine inputs. These processes could occur either in the water column (from sinking particles) or at oxygenated margins. These signatures could then be transported within deep water masses following the oceanic currents described above. Particulate ^{232}Th concentrations (29) combined with particulate Fe concentrations (44) suggest that particulate Fe is dominated by lithogenic Fe along the transect, with a trend toward larger lithogenic fractions at depth compared with the intermediate layers. This supports the likely role played by non-reductive release of DFe from lithogenic particulate Fe within the water column in the deep ocean.

Conclusions

The above discussion leads us to conclude the following:

i) In the intermediate waters, DFe primarily originates from remineralization of organic matter in the water column and the redistribution of this regenerated DFe through mixing, and sediment reductive dissolution at continental margins also related to organic matter remineralization.

ii) In the deeper waters, DFe sources are dominated by abiotic process(es): non-reductive release of DFe from particles, notably lithogenic ones, such as desorption, and/or ligand-promoted dissolution. Iron release from lithogenic particles combined to iron adsorption onto particles (DFe scavenging) may be regarded as iron exchange between both phases, as previously suggested in the North Atlantic and the West Pacific (3, 4). This process could correspond to the reversible scavenging concept developed for thorium and protactinium (5).

Overall, our Fe isotope data unambiguously reveal that the DFe cycling in the intermediate and deep layers of the studied area is dominated by distinct processes and/or external sources. This conclusion could not have been deduced from concentration data only. It goes against the mainstream oversimplified view according to which remineralization of organic matter is the major pathway releasing DFe in the deep ocean (2, 39, 40). Recognition of these differences, found in the Southern Ocean, but which may also occur in other oceanic regions, will have important impacts on models of the oceanic iron cycle and hence on oceanic biogeochemical cycles, the global carbon cycle, and the climate.

More specifically, taking into account the non-reductive release of DFe from particles, notably lithogenic ones, in the deep ocean could have several implications. This would add an additional source to the global oceanic DFe budget. Similarly to what has been proposed for similar processes at ocean margins (45), (*i*) this could shorten the DFe mean oceanic residence time, and (*ii*) these processes could release other elements, including other nutrients and micronutrients. Such iron release processes are likely controlled by different parameters compared with those involved into biologically mediated organic matter remineralization. Particulate iron concentrations, notably lithogenic ones, but also physical and chemical parameters such as mineralogy, temperature, or pH, could influence the magnitude of this DFe source. This suggests that the oceanic DFe budget could be more sensitive than previously thought to continental erosion, particle transport, and dissolved/particle interactions. Finally, as for all deep iron sources, recognition of this deep DFe release from lithogenic particles would reinforce the role played by vertical mixing and deep water upwelling in the control of DFe supply to the surface ocean and therefore in the control of primary production. One could

expect that the influence of these processes on primary production would be maximum in areas where surface DFe inputs are low (HNLC areas) and where deep water upwelling is large, such as in the Southern Ocean.

Sampling and Methods

Sampling and analytical protocols are given in *Supporting Information*. The analytical protocol has been previously published (46), validated by the GEOTRACES intercalibration exercise (47) and an intercomparison study (48).

ACKNOWLEDGMENTS. We are grateful to M. Boye and S. Speich, co-chief scientists of the Bonus/GoodHope cruise. We thank the Go-Flo sampling team, J. Bown, M. Boye, E. Bucciarelli, F. Chever, G. Sarthou, and B. Wake; and the Inductively Coupled Plasma Mass Spectrometry Group of Observatoire Midi-Pyrénées, J. Chmeleff, F. Candaudap, and A. Marquet. We thank the captain and crew of the French R/V *Marion Dufresne*. We thank two anonymous reviewers who helped improving the data interpretation and quality of the manuscript, and Bob Anderson for proofreading. The Region Midi Pyrénées and Pôles de Recherche et d'Enseignement Supérieur funded the PhD fellowship of C.A. Université Paul Sabatier, CNRS, and Institut National des Sciences de l'Univers funded this work.

1. Martin JH, Fitzwater SE (1988) Iron deficiency limits phytoplankton growth in the north-east Pacific subarctic. *Nature* 331:341–343.
2. Boyd PW, Ellwood MJ (2010) The biogeochemical cycle of iron in the ocean. *Nat Geosci* 3(10):675–682.
3. Labatut M, et al. (2014) Iron sources and dissolved-particulate interactions in the seawater of the Western Equatorial Pacific, iron isotope perspectives. *Global Biogeochem Cycles* 28:1044–1065.
4. John SG, Adkins J (2012) The vertical distribution of iron stable isotopes in the North Atlantic near Bermuda. *Global Biogeochem Cycles* 26(2):2034.
5. Bacon MP, Anderson RF (1982) Distribution of thorium isotopes between dissolved and particulate forms in the deep sea. *J Geophys Res* 87(C3):2045–2056.
6. Nozaki Y, Alibo DS (2003) Importance of vertical geochemical processes in controlling the oceanic profiles of dissolved rare earth elements in the northeastern Indian Ocean. *Earth Planet Sci Lett* 205(3-4):155–172.
7. Little SH, Vance D, Siddall M, Gasson E (2013) A modeling assessment of the role of reversible scavenging in controlling oceanic dissolved Cu and Zn distributions. *Global Biogeochem Cycles* 27(3):780–791.
8. Lacan F, et al. (2008) Measurement of the isotopic composition of dissolved iron in the open ocean. *Geophys Res Lett* 35(24):L24610.
9. John SG, Mendez J, Moffett J, Adkins J (2012) The flux of iron and iron isotopes from San Pedro Basin sediments. *Geochim Cosmochim Acta* 93:14–29.
10. Radic A, Lacan F, Murray JW (2011) Isotopic composition of dissolved iron in the equatorial Pacific Ocean: New constraints for the oceanic iron cycle. *Earth Planet Sci Lett* 306:1–10.
11. Conway TM, John SG (2014) Quantification of dissolved iron sources to the North Atlantic Ocean. *Nature* 511(7508):212–215.
12. Severmann S, McManus J, Berelson WM, Hammond DE (2010) The continental shelf benthic iron flux and its isotope composition. *Geochim Cosmochim Acta* 74(14): 3984–4004.
13. Homoky WB, Severmann S, Mills RA, Statham PJ, Fones GR (2009) Pore-fluid Fe isotopes reflect the extent of benthic Fe redox recycling: Evidence from continental shelf and deep-sea sediments. *Geology* 37(8):751–754.
14. Ellwood MJ, et al. (2015) Iron stable isotopes track pelagic iron cycling during a subtropical phytoplankton bloom. *Proc Natl Acad Sci USA* 112(1):E15–E20.
15. Rouxel OJ, Auro M (2010) Iron isotope variations in coastal seawater determined by multicollector ICP-MS. *Geostand Geoanal Res* 34(2):135–144.
16. Chever F, et al. (2015) Total dissolvable and dissolved iron isotopes in the water column of the Peru upwelling regime. *Geochim Cosmochim Acta* 162:66–82.
17. Homoky WB, John SG, Conway TM, Mills RA (2013) Distinct iron isotopic signatures and supply from marine sediment dissolution. *Nat Commun* 4:2143.
18. Beard BL, et al. (2010) Iron isotope fractionation between aqueous ferrous iron and goethite. *Earth Planet Sci Lett* 295(1-2):241–250.
19. Crosby H, Roden E, Johnson C, Beard B (2007) The mechanisms of iron isotope fractionation produced during dissimilatory Fe(III) reduction by *Shewanella putrefaciens* and *Geobacter sulfurreducens*. *Geobiology* 5(2):169–189.
20. Johnson CM, Roden EE, Welch SA, Beard BL (2005) Experimental constraints on Fe isotope fractionation during magnetite and Fe carbonate formation coupled to dissimilatory hydrous ferric oxide reduction. *Geochim Cosmochim Acta* 69(4):963–993.
21. Dideriksen K, Baker JA, Stipp SLS (2008) Equilibrium Fe isotope fractionation between inorganic aqueous Fe(III) and the siderophore complex, Fe(III)-desferrioxamine B. *Earth Planet Sci Lett* 269(1-2):280–290.
22. Kiczka M, et al. (2010) Iron isotope fractionation during proton- and ligand-promoted dissolution of primary phyllosilicates. *Geochim Cosmochim Acta* 74(11):3112–3128.
23. Bown J, et al. (2011) The biogeochemical cycle of dissolved cobalt in the Atlantic and the Southern Ocean south off the coast of South Africa. *Mar Chem* 126(1-4):193–206.
24. Talley LD, Pickard GL, Emery WJ, Swift JH (2011) *Descriptive Physical Oceanography: An Introduction* (Elsevier Academic, Burlington, MA), 6th Ed.
25. Johnson CM, Beard BL, Roden EE (2008) The iron isotope fingerprints of redox and biogeochemical cycling in the modern and ancient Earth. *Annu Rev Earth Planet Sci* 36:457–493.
26. Sarthou G, et al. (2011) Labile Fe(II) concentrations in the Atlantic sector of the Southern Ocean along a transect from the subtropical domain to the Weddell Sea Gyre. *Biogeosciences* 8(9):2461–2479.
27. Talley LD (1999) Some aspects of ocean heat transport by the shallow, intermediate and deep overturning circulations. *Mechanisms of Global Climate Change at Millennial Time Scales*, Geophysical Monograph Series, eds Clark PU, Webb RS, Keigwin LD (American Geophysical Union, Washington, DC), pp 1–22.
28. Carter BR, Talley LD, Dickson AG (2014) Mixing and remineralization in waters detrained from the surface into Subantarctic Mode Water and Antarctic Intermediate Water in the southeastern Pacific. *J Geophys Res Oceans* 119(6):4001–4028.
29. Garcia-Solsona E, et al. (2014) Rare earth elements and Nd isotopes tracing water mass mixing and particle-seawater interactions in the SE Atlantic. *Geochim Cosmochim Acta* 125:351–372.
30. Poitrasson F, et al. (2014) Iron isotope composition of the bulk waters and sediments from the Amazon River Basin. *Chem Geol* 377:1–11.
31. Sarthou G, et al. (2008) The fate of biogenic iron during a phytoplankton bloom induced by natural fertilisation: Impact of copepod grazing. *Deep Sea Res Part II Top Stud Oceanogr* 55(5-7):734–751.
32. Alldredge AL, Cohen Y (1987) Can microscale chemical patches persist in the sea? Microelectrode study of marine snow, fecal pellets. *Science* 235(4789):689–691.
33. Beal LM, Ffield A, Gordon AL (2000) Spreading of Red Sea overflow waters in the Indian Ocean. *J Geophys Res* 105(C4):8549–8564.
34. Moffett JW, et al. (2015) Biogeochemistry of iron in the Arabian Sea. *Limnol Oceanogr* 60(5):1671–1688.
35. Measures CI, et al. (2013) The influence of shelf processes in delivering dissolved iron to the HNLC waters of the Drake Passage, Antarctica. *Deep Sea Res Part II Top Stud Oceanogr* 90:77–88.
36. Hegner E, Dauelsberg HJ, van der Loeff MMR, Jeandel C, de Baar HJW (2007) Nd isotopic constraints on the origin of suspended particles in the Atlantic sector of the Southern Ocean. *Geochem Geophys Geosyst* 8:Q10008.
37. Boye M, et al. (2012) Distributions of dissolved trace metals (Cd, Cu, Mn, Pb, Ag) in the southeastern Atlantic and the Southern Ocean. *Biogeosciences* 9(8):3231–3246.
38. Chever F, et al. (2010) Physical speciation of iron in the Atlantic sector of the Southern Ocean along a transect from the subtropical domain to the Weddell Sea Gyre. *J Geophys Res* 115(C10):2156–2202.
39. Wu J, Boyle E (2002) Iron in the Sargasso Sea: Implications for the processes controlling dissolved Fe distribution in the ocean. *Global Biogeochem Cycles* 16(4):33-1–33-8.
40. Bruland KW, Orians KJ, Cowen JP (1994) Reactive trace metals in the stratified central North Pacific. *Geochim Cosmochim Acta* 58:3171–3182.
41. Boyd PW, Ibisanmi E, Sander SG, Hunter KA, Jackson GA (2010) Remineralization of upper ocean particles: Implications for iron biogeochemistry. *Limnol Oceanogr* 55(3):1271–1288.
42. Brantley SL, et al. (2004) Fe isotopic fractionation during mineral dissolution with and without bacteria. *Geochim Cosmochim Acta* 68(15):3189–3204.
43. Revels BN, Ohnemus DC, Lam PJ, Conway TM, John SG (2014) The isotope signature and distribution of particulate iron in the north Atlantic ocean. *Deep Sea Res Part II Top Stud Oceanogr* 116:321–331.
44. Mawji E, et al. (2015) The GEOTRACES Intermediate Data Product 2014. *Mar Chem* 177(Pt 1):1–8.
45. Jeandel C, et al. (2011) Ocean margins: The missing term in oceanic element budgets? *Eos (Wash DC)* 92(26):217–218.
46. Lacan F, et al. (2010) High-precision determination of the isotopic composition of dissolved iron in iron depleted seawater by double spike multicollector-ICPMS. *Anal Chem* 82(17):7103–7111.
47. Boyle EA, et al. (2012) GEOTRACES IC1 (BATS) contamination-prone trace element isotopes Cd, Fe, Pb, Zn, Cu, and Mo intercalibration. *Limnol Oceanogr Methods* 10: 653–665.
48. Conway TM, John SG, Lacan F (2016) Intercomparison of dissolved iron isotope profiles from reoccupation of three GEOTRACES stations in the Atlantic Ocean. *Mar Chem* 183:50–61.
49. Poitrasson F (2006) On the iron isotope homogeneity level of the continental crust. *Chem Geol* 235(1-2):195–200.
50. Beard BL, Johnson CM, Von Damm KL, Poulson RL (2003) Iron isotope constraints on Fe cycling and mass balance in oxygenated Earth oceans. *Geology* 31(7):629–632.
51. Escoube R, et al. (2015) Iron isotope systematics in Arctic rivers. *C R Geosci* 347(7-8): 377–385.
52. Rouxel O, Sholkovitz E, Charette M, Edwards KJ (2008) Iron isotope fractionation in subterranean estuaries. *Geochim Cosmochim Acta* 72(14):3413–3430.
53. Rouxel O, Shanks WC, III, Bach W, Edwards KJ (2008) Integrated Fe- and S-isotope study of seafloor hydrothermal vents at East Pacific Rise 9–10°N. *Chem Geol* 252(3-4): 214–227.
54. Sokolov S, Rintoul SR (2009) Circumpolar structure and distribution of the Antarctic Circumpolar Current fronts: 2. Variability and relationship to sea surface height. *J Geophys Res* 114(C11):C11019.
55. Schlitzer R (2009) *Ocean Data View*. Available at odv.awi.de. Accessed November 3, 2013.